Self-Organized Origami

L. Mahadevan[1]* and S. Rica[2]

The controlled folding and unfolding of maps, space structures, wings, leaves, petals, and other foldable laminae is potentially complicated by the independence of individual folds; as their number increases, there is a combinatorial explosion in the number of folded possibilities. The artificially constructed Miura-ori (*1*) pattern, with a periodic array of geometrically and elastically coupled mountain and valley folds (Fig. 1A), circumvents this complication by allowing the entire structure to be folded or unfolded simultaneously. Making such a pattern is not easy, so it may be surprising to find an elegant natural counterpart that is a few hundred millennia old. In Fig. 1B, we show the different stages of the opening of a hornbeam leaf that starts life in its bud as a Miura-ori folded pattern (*2*). Similar structures arise in insect wings (*3*) and elsewhere in nature (*4*), suggesting that these origami patterns are a result of convergent design. This raises a question of mechanism: How might this spatial organization of folds be brought about?

In Fig. 1C, we show the realization of a simple physical solution to this question. The biaxial compression of a thin, stiff, elastic film (with Young's modulus E, Poisson ration ν, thickness h, and size $L \gg h$) supported on a thick, soft substrate (with Young's modulus $E_p \ll E$ and thickness $H \gg h$) yields into a Miura-ori pattern without any external guidance other than that induced by relatively benign, isotropic, compressive strains that arise because of the relative expansion and contraction between the film and substrate induced by thermal (*5*) or desiccating (*6*) effects. Initially, we get primary buckles with wavelength $\lambda \sim h(E/E_p)^{1/3}$ (*5*), which is very small compared to the lateral extent of the system. However, at the onset of the instability, these straight primary buckles do not have any preferred orientation in a large system and instead form large uncorrelated patches. Nonlinear deformations of these primary buckles, through global compression or extension parallel or perpendicular to their orientation, lead to modulational instabilities wherein the buckles collectively deform through soft modes, which are energetically cheaper than the local extension or compression of individual buckles (supporting online text). Thus, the Miura-ori pattern is just the natural response of a softly supported stiff skin to weak compression along the primary buckles (or weak extension perpendicular to them), wherein the buckles tilt into a zigzag pattern separated by kinks.

Quantifying this through a mathematical analysis of the equations of elasticity (supporting online text) away from the onset of the instability leads to the Newell-Whitehead-Segel equation (*7*, *8*) for the complex-valued amplitude $A(x,y)$

$$\varepsilon A + \frac{h^2}{12(1-\nu^2)} \times (\partial_x - \frac{i}{2k_c}\partial_{yy})^2 A - g|A|^2 A = 0 \quad (1)$$

Here $Re[A(x,y)e^{ik_c x}]$ is the vertical deflection of the skin, $k_c = 2\pi/\lambda$ is the wave number at onset, ε characterizes the distance from the instability threshold, and g characterizes the saturation amplitude. The form of Eq. 1 follows from symmetry considerations (supporting online text) and describes a variety of planform patterns, including the zigzag patterns found in fluid convection, superconductivity, liquid crystals, etc. Our interpretation in the context of folding patterns suggests that Eq. 1 also provides a natural mathematical framework for the self-organization of Miura-ori. Indeed, a numerical simulation of Eq. 1 in a rectangular domain with periodic boundary conditions in one direction and Neumann conditions in an orthogonal direction reproduces the Miura-ori patterns with creases of wavelength λ (Fig. 1D).

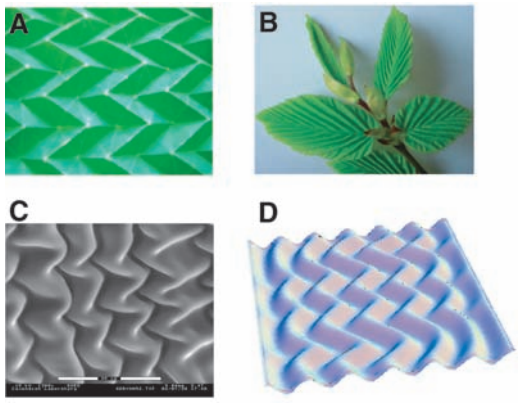

Fig. 1. (**A**) Plan view of a paper Miura-ori pattern (size, 5 cm), showing the periodic mountain-valley folds. The sharp re-entrant creases that come together at kinks allow the whole structure to fold or unfold simultaneously. (**B**) Hornbeam leaves (length, 5 cm) in the process of blooming show a natural occurrence of Miura-ori. A single row of kinks along the midrib allows a folded leaf to be deployed once the bud opens (*2*), as seen in the different stages of leaf opening (clockwise from the top). (**C**) Zigzag Miura-ori patterns in a thin film atop a thick elastic substrate that is compressed biaxially manifest here in a drying slab of gelatin with a thin skin that forms naturally (*6*), showing the physically driven self-organization of Miura-ori. Scale bar, 35 μm. (**D**) Simulations of Eq. 1 yield Miura-ori patterns that arise as a modulational instability of the primary (straight) wrinkles (supporting online text).

Although Eq. (*1*) is asymptotically valid only in the weakly nonlinear regime, in practice it describes the patterns well even far from the onset of the zigzag folds. Additionally, the strong localization of the creases and kinks follows naturally from the nonlinear evolution of the pattern in light of the small thickness of the skin-like upper film and the softness of the substrate, leading to almost isometric mountain-valley fold patterns (Fig. 1, A and C). The size d of the kinks is determined by minimizing the sum of the kink-bending energy $U_K \sim Eh^3\ln(R/d)$, due primarily to conical bending of the thin sheet of size R, and the additional energy of deforming the attached substrate below the kinks, $U_s \sim E_p d^3$. This yields $d \sim h(\frac{E}{E_p})^{1/3} \sim \lambda$, consistent with observations (Fig. 1C).

Our observations and analysis provide a mechanism for naturally occurring Miura-ori. Stresses induced by the relative growth of stiff skins on soft supports will spontaneously fold into structures such as those shown in Fig. 1; stress-mediated apoptosis may then separate the skin from the tissue to form deployable laminae such as leaves and insect wings.

References and Notes

1. K. Miura, *Proceedings of the 31st Congress of the International Astronautical Federation*, IAF-80-A 31, (American Institute for Aeronautics and Astronautics, New York, 1980), pp. 1–10.
2. H. Kobayashi, B. Kresling, J. Vincent, *Proc. R. Soc. London Ser. B.* **265**, 147 (1998).
3. F. Haas, R. W. Wooton, *Proc. R. Soc. London Ser. B.* **263**, 1651 (1996).
4. B. Kresling, *Biomimetics* **3**, 105 (1991).
5. N. Bowden, S. Brittain, A. G. Evans, J. Hutchinson, G. Whitesides, *Nature* **393**, 146 (1998).
6. R. Rizzieri, personal communication.
7. L. A. Segel, *J. Fluid Mech.* **38**, 203 (1969).
8. A. C. Newell, J. Whitehead, *J. Fluid Mech.* **38**, 279 (1969).
9. L.M. acknowledges support from the Harvard Materials Research Science and Engineering Center and the Office of Naval Research Young Investigator Program; S.R. acknowledges support from Fondo de Ciencia y Tecnologia (FONDECYT), Chile.

[1]Division of Engineering and Applied Sciences and Department of Organismic and Evolutionary Biology, Harvard University, Cambridge, MA 02138, USA. [2]Departamento de Fisica, Universidad de Chile, Blanco Encalada 2008, Santiago, Chile.

*To whom correspondence should be addressed. E-mail: lm@deas.harvard.edu

Supplementary Online Material for "Self-organized Origami"

L. Mahadevan and S. Rica

Understanding the process of Miura-ori patterning requires a weakly nonlinear analysis of the straight dimensional periodic buckling pattern in the neighborhood of the primary instability that selects a preferred wavelength, but no preferred direction. In a large system, i.e. one where the wavelength of the primary pattern is small compared to the size of the system, tensile stresses along the buckles (or equivalently compression perpendicular to them) lead to the so-called Eckhaus instability, wherein a localized defect arises because it is easier for the buckles to respond to a weak expansion by localizing the deformation rather than accommodating it over the entire domain. On the other hand, compressive stresses along the buckles (or equivalently tension perpendicular to them) lead to the so-called zigzag instability which arises as a consequence of the fact that zigzag patterns allow for the accommodation of the effective lateral expansion of the buckles without changing the wavelength, but by simply tilting the folds; however since the folds can tilt in one of two equivalent directions, the most natural response of the system is to alternate the tilted regions to accommodate the lateral expansion at the expense of introducing localized defects. Our arguments so far are based on simple dimensional and geometric considerations. Indeed these instabilities of one-dimensional cellular patterns are independent of the detailed mechanisms at work and have been observed in other physical systems such as fluid convection, liquid crystals, superconductivity, flames etc. and reflect only the underlying symmetries of the system and the way in which they are broken (S1).

In the specific case of interest here, since the sheet is attached to a soft substrate, delamination does not occur and the deformations of the substrate are slaved to those of

the sheet. In the bulk the polymer substrate satisfies the equations of elastic equilibrium. Assuming that the polymer is isotropic and linearly elastic, with Young's modulus E_p, Poisson ratio ν_p and depth l we may then write (S2)

$$\Delta u_i + \frac{1}{1-2\nu_p}\partial_i(\partial_k u_k) = 0 \tag{1}$$

where $u_i(x,y,z)$ are the displacements of the polymer. At the base of the polymer of thickness l, we assume that $u_i(x,y,-l) = 0$. At the interface with the thin stiff skin of thickness $h(<<l)$, Young's modulus E, and Poisson ratio ν, the continuity of traction and displacement implies that

$$\begin{aligned} E\hbar^2\Delta^2\varsigma - \partial_\alpha(\sigma_{\alpha\beta}\partial_\beta\varsigma) &= \frac{p_z}{h} \\ \partial_\alpha\sigma_{\alpha\beta} &= \frac{p_\beta}{h} \end{aligned} \tag{2}$$

Here $u_3(x,y,0) = \varsigma(x,y)$ is the out-of-plane deformation, $\sigma_{\alpha\beta}(x,y)$ is the two-dimensional in-plane stress field in the plate, $\hbar^2 = h^2/12(1-\nu^2)$, and p_β, p_z are the in-plane and out-of-plane components of the tractions at the polymer-skin interface. In fact Eq. (2) are the Foppl- von Karman equations (S2) that are valid for the geometrically nonlinear deformations of a plate. Seeking linear periodic perturbation solutions to Eq. (1)-(2) of the form: $\varsigma(x,y) = A_k e^{i(k_x x + k_y y)} + A_k^* e^{-i(k_x x + k_y y)}$ where A_k is the amplitude and (k_x,k_y) is the two-dimensional wave-vector of the perturbation with wave-number $k = (k_x^2 + k_y^2)^{1/2}$, we find that the curve of marginal stability describing the in-plane compressive stress at the onset of the buckling instability $\sigma_{\alpha\beta} = -\sigma_c \delta_{\alpha\beta}$ is given by

$$\frac{\sigma_c}{E} = (k\hbar)^2 + \frac{E_p(1-\nu_p)}{E(1+\nu)}\frac{(2kl + (3-4\nu_p)\sinh(2kl)}{kh[-k^2l^2 + (3-4\nu_p)^2\sinh^2(kl)]} \tag{3}$$

If the compressive stress is larger than the value given by Eq. (3) A_k is nonzero, and the flat state exchanges stability with the periodic one. In the limit when the substrate is very deep so that $kl >> 1$, the most unstable wavenumber is given by minimizing Eq. (3) and yields the relation $k_c h = [\frac{12(1-\nu_p)(1-\nu^2)}{(1+\nu_p)(3-4\nu_p)}]^{1/3}(\frac{E_p}{E})^{1/3}$, so that the critical wavelength at onset $\lambda_c = \frac{2\pi}{k_c} \sim h(\frac{E}{E_p})^{1/3}$. When the applied stress exceeds that at onset of the primary buckling instability, i.e. $\sigma = \sigma_c + \delta\sigma_c$, with $\delta\sigma_c \sim \varepsilon\sigma_c$, a band of wave-numbers around the most unstable one are excited, as shown in Figure S1(a); the width of this band scales as $\delta k_c \sim \varepsilon^{1/2} k_c$, as a simple consequence of geometry. In Fig. S1(b), we see that if we assume that the primary instability at some location has a wave-vector oriented in the x-direction, the band of excited wave-numbers in the x-direction of width $\delta k_x \sim \varepsilon^{1/2} k_c$ leads to a band of excited wave-numbers in the y-direction of width $\delta k_y \sim \varepsilon^{1/4} k_c$, which again follows from simple geometry. We thus see that above the onset of the primary instability, interactions between the excited band of wave-numbers leads to modulational instabilities on very long wavelengths of order O($\varepsilon^{-1/4}$). The shape of the transition curve, or equivalently the linearized operator in the vicinity of the instability may then be written as[1] $M = \varepsilon - (k - k_c)^2 \hbar^2$, with $k = [(k_c + \delta k_x)^2 + \delta k_y{}^2]^{1/2}$. Expanding the previous expression and keeping only the leading order terms in δk_x and δk_y yields $M = \varepsilon - (\delta k_x + \frac{1}{2}\frac{\delta k_y^2}{k_c})^2 \hbar^2$. Finally, using the substitution $\delta k_x \to -i\partial_x A$, $\delta k_y \to -i\partial_y A$, and noting that the nonlinear term follows from the phase invariance of the pattern under the transformation of the amplitude $A \to A e^{i\phi_0}$, then allows us obtain the equation for the complex-valued amplitude $A(x, y)$

$$\varepsilon A + \hbar^2(\partial_x - \frac{i}{2k_c}\partial_{yy})^2 A - g|A|^2 A = 0 \qquad (4)$$

which is well-known as the Newell-Whitehead-Segel equation (S3,S4). Here ε is proportional to the distance to the threshold of the instability and g characterizes the saturation amplitude. Eq. (4) describes the weakly nonlinear behavior of the primary buckling pattern, and indeed provides a generic description of long wavelength modulations of cellular patterns (S1). Although a formal calculation will lead to the explicit dependence of g on the problem parameters, this is of no relevance to the onset of the zigzag or the modulational instability[1].

A numerical simulation of Eq. (4) with periodic boundary conditions in one direction and Neumann conditions in another in a rectangular domain using a linear relaxation dynamics is shown in Fig. S1(c) and confirms the occurrence of the zigzag instability when the primary wrinkles are weakly compressed, with a series of defects or kinks corresponding to zones of double curvature. In Fig. S1(d) we show the Eckhaus instability when the wrinkles are weakly extended and in Fig. S1(e), we show the effect of a hole or other relief structure in the thin film which softens the folds in its vicinity as documented in earlier experiments (S5). In all these simulations, the strong localization of the kinks is evident, and shows how the large disparity between the energetics of bending and stretching a thin sheet favours the concentration of curvature which is energetically inexpensive. Of course Eq. (4) is no longer valid in such a region and we have to resort to a more complete description that accounts for the geometrical nonlinear behavior of the thin film (S6). Indeed, very recent work (S7, S8) shows that in the presence of external constraints, numerical simulations of Eq. (1)-(2) are able to reproduce some of these fine-scale features in complex wrinkling patterns, complementing the current work on the long wavelength features of the pattern.

References:

S1. Cross, M. and Hohenberg, P. (1993) Rev. Mod. Phys., **65**, 854-1112.

S2. Landau, L. and Lifshitz, E. (1986) Theory of Elasticity, 3rd edn., Pergamon (NY).

S3. Segel, L.A. (1969), J. Fluid Mech., 38, 203-235.

S4. Newell, A.C. and J. Whitehead (1969), J. Fluid Mech., 38, 279-303

S5. Bowden, N., S. Brittain, A.G. Evans, J. Hutchinson and G. Whitesides (1998), Nature, 393, 146-50.

S6. Cerda, E. and L. Mahadevan (1998) Phys. Rev. Lett., **80**, 2358-61.

S7. Xia, C. and J. Hutchinson (2004), ASME J. Appl. Mech. , **71,** 597-603.

S8. Huang, Z., W. Hong and Z. Suo (2004), PRE, **71**,030601(R).

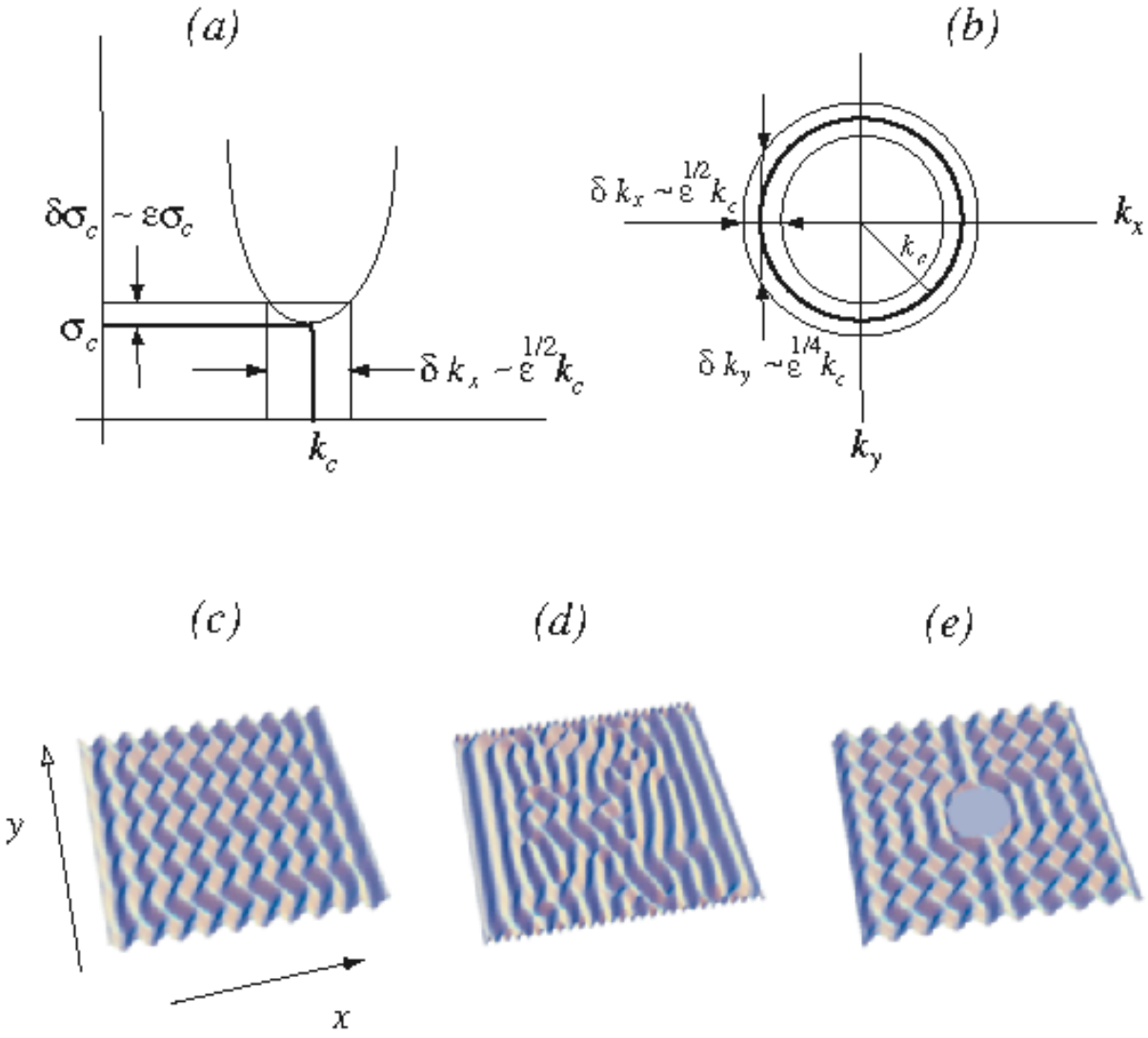

Figure S1

(A) The stability diagram showing the finite wavenumber buckling instability corresponding to a critical stress σ_c for which a critical wavenumber $k_c \sim h^{-1}(E_p/E)^{1/3}$ is selected. The supercritical nature of the instability immediately characterizes the scaling behavior for the band of wavenumbers

excited when the stress is slightly larger than that required for the onset of the instability.

(B) The long wavelength modulational instability in the y-direction follows directly from the consideration of modulations of the primary instability, here assumed to be in the x-direction.

Numerical simulations (C,D,E) of (4) are done with periodic boundary conditions in the y-direction and Neumann boundaries in the x-direction. The simulations were carried out on a 128 x 128 grid with a spacing $h\varepsilon^{-1/2}$, and scaling the amplitude A by $(\varepsilon/g)^{1/2}$. For all simulations we set $k_c = 0.6\ \varepsilon^{1/2}/h$. We start the simulation with the amplitude $A(x,y) = ((\varepsilon - q^2)/g)^{1/2}\, e^{iqx}$ where a weak tensile stress perpendicular to the wrinkles corresponds to $q<0$ (or equivalently a weak compressive stress along them), and evolve this initial condition using a relaxation scheme. A weak compressive stress, on the other hand corresponds to $q>0$ along the wrinkles (or equivalently a weak tensile stress perpendicular to them).

(C) Numerical simulation shows the occurrence of the zigzag instability. Here the mismatch $q = -0.1\ \varepsilon^{1/2}/h$ corresponds to a weak tensile stress perpendicular to the wrinkles.

(D) Numerical simulation of (4) with $q = 0.75\ \varepsilon^{1/2}/h$ shows the occurrence of the Eckhaus instability, corresponding to a weak compressive stress perpendicular to the wrinkles, or equivalently, a weak tensile stress along them.

(E) Numerical simulation of (4) with $q = -0.15\ \varepsilon^{1/2}/h$ shows how the zigzag instability is modified in the presence of a hole or other relief structure where we assume that the amplitude A vanishes, i.e. we have a Dirichlet boundary condition.